

# Morphology transitions induced by chemotherapy in carcinomas “in situ”

S. C. Ferreira Jr.\*

*Departamento de Física, Instituto de Ciências Exatas, Universidade Federal de Minas Gerais,  
Caixa Postal 702, 30161-970 Belo Horizonte, Minas Gerais, Brazil*

M. L. Martins†

*Departamento de Física, Universidade Federal de Viçosa, 36571-000, Viçosa, Minas Gerais, Brazil*

M. J. Vilela‡

*Departamento de Biologia Animal, Universidade Federal de Viçosa, 36571-000, Viçosa, Minas Gerais, Brazil*

(Dated: November 15, 2018)

Recently, we have proposed a nutrient-limited model for the avascular growth of tumors including cell proliferation, motility and death [1], that, qualitatively reproduces commonly observed morphologies for carcinomas *in situ*. In the present work, we analyze the effects of distinct chemotherapeutic strategies on the patterns, scaling and growth laws obtained for such nutrient-limited model. Two kinds of chemotherapeutic strategies were considered, namely, those that kill cancer cells and those that block cell mitosis but allows the cell to survive for some time. Depending on the chemotherapeutic schedule used, the tumors are completely eliminated, reach a stationary size or grow following power laws. The model suggests that the scaling properties of the tumors are not affected by the mild cytotoxic treatments, although a reduction in growth rates and an increase in invasiveness are observed. For the strategies based on antimitotic drugs a morphological transition in which compact tumors become more fractal under aggressive treatments was seen.

PACS numbers: 87.19+e, 87.18.Hf, 87.18.Bb, 87.15.Vv

## I. INTRODUCTION

Cancer is the uncontrolled cellular growth in which neoplastic cells invade adjacent normal tissues and give rise to secondary tumors (metastasis) on tissues or organs distant from its primary origin [2]. A cancer that remains confined within a messed surface, without break of the underlying basement membrane, is referred to as carcinoma “in situ”. “In situ” carcinoma is characterized by intense cytological atypia, necrosis, and frequent and abnormal mitosis, the tumor cells being arranged in various distinctive patterns [3]. A malignant tumor is derived from a single cell that, years before the tumor becomes clinically detectable, began an inappropriate pathway of proliferation [4]. Although cancers are extremely diverse and heterogeneous, a small number of pivotal steps associated to both deregulated cell proliferation and suppressed cell death are required for the development of any and all tumors. Indeed, all neoplasms evolve accordingly to an universal scheme [5, 6]. In the struggle against cancer, surgical removal, chemotherapy and/or radiotherapy are the most commonly used treatment for the complete eradication of the tumor mass. Nowadays, new approaches, such as immunotoxins [7], gene [8], anti-angiogenic [9] and virus [10] therapies, are being developed and have been successfully used in the treatment of

several kinds of experimental and human tumors.

Mathematical models are always used as a tentative for describing cancer growth. In particular, numerous models based on classical reaction-diffusion equations have been proposed to investigate the growth of tumor spheroids [11], cancer progress and its interaction with the immune system [12], and the tumor angiogenesis [13, 14]. Fractal growth patterns in gliomas (brain tumors) were recently investigated by Sander and Deisboeck [15]. Scalerandi *et. al.*, using the local interaction simulation approach (LISA), formulated models for the evolution of avascular tumors [16] and tumor cords [17] under nutrient competition. They also analyzed the effects of tumor vascularization [18] on cancer growth. Recently, we have studied a diffusion-limited model for the growth of carcinomas “in situ” in which cell proliferation, motility and death are locally controlled by growth factors [19, 20]. This model generates compact, connected and disconnected morphologies characterized by Gompertzian growth in time and distinct scaling laws for the tumor interfaces. In order to generate papillary and ramified morphologies found in many epithelial cancers and trichoblastomas, we were led to analyze the effects of nutrient competition in cancer development [1].

In addition to the vast literature dedicated to tumor growth modeling, many research papers addressing cancer therapies have recently been published. Indeed, cancer cell kinetics under treatments using antimitotic agents [21, 22], radiotherapy [23], virus that replicate selectively in tumor cells [24], anti-angiogenic chemicals [25], as wells as the effects of tumor drug resistance and tumor vasculature on chemotherapies [26], were studied

---

\*Electronic address: silviojr@fisica.ufmg.br

†Electronic address: mmartins@ufv.br

‡Electronic address: marcelo@ufv.br

using mathematical models.

In this paper it is analyzed the effects of distinct chemotherapeutic strategies in the model for the growth of avascular tumors proposed by us [1]. Specifically, we are interested in possible changes in the tumor patterns, scaling and growth laws reported on the original model triggered by chemotherapies. The paper is organized as follows. In section II the nutrient-limited model for cancer growth and its main results are reviewed. In section III, chemotherapeutic treatments that aim to kill cancer cells are introduced in the framework of the present model and their effects discussed. In section IV, a model for chemotherapy with antimitotic agents is considered. Finally, we draw some conclusions in section V.

## II. THE NUTRIENT-LIMITED MODEL

Our nutrient-limited model combines macroscopic reaction-diffusion equations, describing the nutrient field concentration, with microscopic stochastic rules governing the actions of individual tumor cells. The basic principles included in the model are cell proliferation, motility and death as well as competition for nutrients among cancer and normal cells. Also, the nutrient concentration field locally controls cell division, migration and death.

### A. The model

#### 1. The tissue

The tissue, represented by a square lattice of size  $(L + 1) \times (L + 1)$  and lattice constant  $\Delta$ , is fed by a single capillary vessel at  $x = 0$ , the top of the lattice. The capillary is the unique source from which nutrients diffuse through the tissue towards the individual cells. Although a tumor mass is composed of different cell subpopulations [5], the model considers only three types: normal, cancer and tumor dead cells. Any site, with coordinates  $\vec{x} = (i\Delta, j\Delta)$ ,  $i, j = 0, 1, 2, \dots, L$ , is occupied by only one of these cell types. In contrast to the normal cells, one or more cancer cells can pile up in a given site. In turn, dead tumor cells are inert. Thus, each lattice site can be thought of as a group of cells in which the normal, dead and cancer cell populations assume one of the possible values  $\sigma_n(\vec{x}) = \sigma_d(\vec{x}) = 0, 1$  and  $\sigma_c(\vec{x}) = 0, 1, 2, \dots$ , respectively. Accordingly the theory of the monoclonal origin of cancer [4], a single cancer cell at  $y = L\Delta/2$  and at a distance  $X$  from the capillary is introduced in the normal tissue. Periodic boundary conditions along the horizontal axis are used. The row  $i = 0$  represents the capillary vessel and the sites with  $i = L + 1$  constitute the external border of the tissue. This geometry is particularly adequate to describe the growth of carcinomas (epithelial tumors) “in situ” because the present model consider that the tumor mass receive nutrients only by diffusion from the capillary vessel. However, the model

can be extended to others cancers.

#### 2. The nutrients

The nutrients are divided into two classes: essential to cell proliferation, those necessary to DNA synthesis, and nonessential to cell division. The essential and nonessential nutrients are described by the concentration fields  $N(\vec{x}, t)$  and  $M(\vec{x}, t)$ , respectively. These nutrient fields obey the dimensionless diffusion equations (see ref. [1] for the complete variable transformations)

$$\frac{\partial N}{\partial t} = \nabla^2 N - \alpha^2 N \sigma_n - \lambda_N \alpha^2 N \sigma_c \quad (1)$$

and

$$\frac{\partial M}{\partial t} = \nabla^2 M - \alpha^2 M \sigma_n - \lambda_M \alpha^2 M \sigma_c \quad (2)$$

in which differentiated nutrient consumption rates for normal and cancer cells by factors  $\lambda_N$  and  $\lambda_M$  are assumed. It is important to notice that the model admits the simplest form for nutrient diffusion, i. e., linear equations with constant coefficients. Also,  $\lambda_N > \lambda_M$  is used, reflecting the larger affinity of cancer cells for essential nutrients.

The boundary conditions satisfied by the normalized nutrient concentration fields are  $N(x = 0) = M(x = 0) = 1$ , representing the continuous and fixed supply of nutrients provided by the capillary vessel;  $N(y = 0) = N(y = L)$  and  $M(y = 0) = M(y = L)$ , corresponding to the periodic boundary conditions along the y-axis; at last, Neumann boundary conditions,  $\partial N(x = L)/\partial x = \partial M(x = L)/\partial x = 0$ , are imposed to the border of the tissue.

#### 3. Cell dynamics

In our original model, each tumor cell, randomly selected with equal probability, can carry out one of three actions: division, migration or death. However, in the present work we consider just the accommodation that happens during cell mitosis among the daughter cells. Consequently, each tumor cell can carry out one of two actions.

1. *Division.* Cancer cells divide by mitosis with probability  $P_{div}$ . If the chosen cell is inside the tumor, its daughter will pile up at that site, and  $\sigma_c(\vec{x}) \rightarrow \sigma_c(\vec{x}) + 1$ . Otherwise, if the selected cell is on the tumor border, its daughter cell will occupy at random one of their nearest neighbor sites  $\vec{x}'$  containing a normal or a necrotic cell and, therefore,  $\sigma_c(\vec{x}') = 1$  and  $\sigma_{n,d}(\vec{x}') = 0$ . The mitotic probability  $P_{div}$  is determined by the concentration per cancer cell of the essential nutrients  $N$  present on

the microenvironment of the selected cell:

$$P_{div}(\vec{x}) = 1 - \exp \left[ - \left( \frac{N(\vec{x})}{\sigma_c(\vec{x}) \theta_{div}} \right)^2 \right]. \quad (3)$$

The Gaussian term is included in order to produce a sigmoid curve saturated to the unity, and the model parameter  $\theta_{div}$  controls the shape of this sigmoid.

2. *Death.* Cancer cells die with probability  $P_{del}$ . Thus,  $\sigma_c(\vec{x}) \rightarrow \sigma_c(\vec{x}) - 1$  and  $\sigma_d(\vec{x}) = 1$  when  $\sigma_c$  vanishes. The cell death probability  $P_{del}$  is determined by the concentration per cancer cells of the nonessential nutrients  $M$  present on the microenvironment of the selected cell:

$$P_{del}(\vec{x}) = \exp \left[ - \left( \frac{M(\vec{x})}{\sigma_c(\vec{x}) \theta_{del}} \right)^2 \right], \quad (4)$$

- i. e., a Gaussian distribution whose variance depends on the model parameter  $\theta_{del}$ .

The biological basis for these cell dynamic rules can be found in reference [1]. However, it is worthwhile to notice that from the point of view of the so-called kinetic cellular theory, which provides a general framework for the statistical description of the population dynamics of interacting cells [12], the local probabilities  $P_{div}$  and  $P_{del}$  can be thought as an effective kinetic cellular model.

#### 4. Computer implementation

The growth model simulations were implemented using the following procedure. At each time step  $T$ , Eqs. (1) and (2) are numerically solved in the stationary state ( $\partial N/\partial t = \partial M/\partial t = 0$ ) through relaxation methods. Provided the nutrient concentration at any lattice site,  $N_C(T)$  cancer cells are sequentially selected at random with equal probability. For each one of them, a tentative action (division or death) is randomly chosen with equal probability and the time is incremented by  $\Delta T = 1/N_C(T)$ . The selected cell action will be implemented or not according to the correspondent local probabilities determined by Eqs. (3) or (4). At the end of this sequence of  $N_C(T)$  tentatives, a new time step begins and the entire procedure (solution of the diffusion equations and application of the cell dynamics) is iterated. The simulations stop if any tumor cell reaches the capillary vessel.

### B. Main results

The model reproduces commonly observed tumor morphologies including the papillary, compact and ramified patterns shown in Fig. 2. The nutrient consumption by

normal and cancer cells, controlled by the model parameters  $\alpha$ ,  $\lambda_N$  and  $\lambda_M$ , plays a central role in morphology selection. For small values of these parameters, corresponding to growth conditions in which individual cells demand small nutrient supplies, the patterns tend to be compact and circular (Fig. 2a). However, if the mitotic rate of cancer cells is small due to the large amount of nutrients demanded for cell division, generating a significant competition for nutrients, these compact patterns progressively assume papillary-like morphologies (Fig. 2b). At high nutrient consumption rates these papillary patterns become the rule and, for low cancer cell division, continuously transform into thin tips, filaments or chords of cells (Fig. 2c). Also, the model generates patterns with a inner core of died cells for high nutrient consumption or cell division rates (Fig. 2d). As observed in ‘‘in vivo’’ tumors and ‘‘in vitro’’ multicell spheroids [11], these simulated patterns consist of three distinct regions: a central necrotic core, an inner rim of quiescent cancer cells and a narrow outer shell of proliferating cells.

The tumor patterns generated by our nutrient-limited model were characterized by its gyration radius  $R_g$ , total number of cancer cells  $N_C$ , and number of sites on tumor periphery  $S$  (including the surface of holes, if any). The gyration radius  $R_g$  is defined as

$$R_g = \left( \frac{1}{n} \sum_{i=1}^n r_i^2 \right)^{1/2} \quad (5)$$

where  $n$  is the number of sites occupied by the pattern (cancer or necrotic cells) and  $r_i$  is the distance of the occupied site  $i$  from the tumor mass center. These quantities could be related to clinically important criteria such as progress curves, growth rates (volumetric doubling time) at given radii, proliferative and necrotic fractions of the tumor.

The progress in time of cancer cell populations for all the simulated patterns follows Gompertz curves,

$$N_C(T) = A \exp [- \exp (-k(T - T_c))], \quad (6)$$

representing an initial exponential growth that is saturated in larger times.

Alternatively, as a function of the number of sites occupied by the pattern  $n$ , both  $R_g$  and  $S$  obey power law scalings given by  $R_g \sim n^\nu$  and  $S \sim n^\sigma$ , respectively. For solid patterns these exponents are  $\nu \sim 0.5$  and  $\sigma \sim 0.5$ , corresponding to effective circular and non fractal patterns. As the nutrient consumption increases, the patterns tend to papillary-like shapes for which the exponent  $\sigma$  increases towards the value 1 and the exponent  $\nu$  varies in the range [0.50, 0.60], indicating a fractal morphology for the tumor.

### III. CYTOTOXIC CHEMOTHERAPEUTIC DRUGS

The primary aim of the antitumoral treatment with chemotherapeutic drugs is to kill or at least to stop the proliferation of the cancer cells. In general, the drugs should act only on proliferating cells, mainly the cancer ones. However, drugs also destroy proliferating normal cells promoting several collateral effects [27]. Indeed, epithelial cells from the respiratory and gastro-intestinal systems, which frequently reproduce in order to substitute their dead counterparts, are strongly affected. In this section, we analyze a simple chemotherapeutic model in which the complex details of the cell-cycling responses to the drugs are taking into account by an effective kinetic model.

#### A. The model

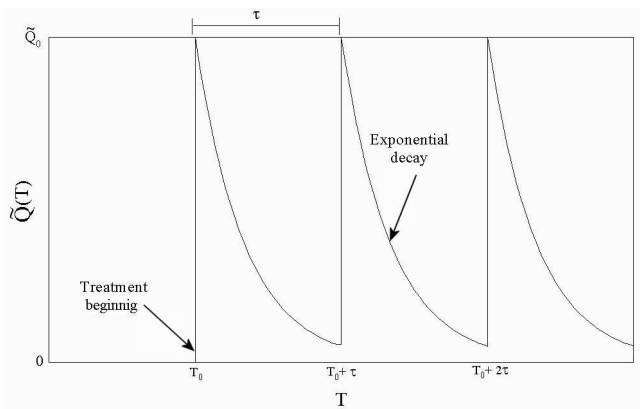


FIG. 1: Temporal profile of drugs concentration at the capillary vessel.

As used in previous works [28], the chemotherapy is modelled by a periodic delivery of cytotoxic drugs through the same capillary vessel supplying the nutrients to the tissue. Several cytotoxic drugs and their properties were exhaustively studied such as amsacrine, cisplatin, cyclophosphamide, cytarabine, mustine, and anthracycline [29]. Here, the numerous barriers involved in tumor drug delivery [30] were not considered, and the treatment begins when the tumor mass contains  $N_0$  cancer cells. When a dose is applied, the drug concentration in the capillary assumes a value  $\tilde{Q}_0$ . By hypothesis, this concentration level decays exponentially in time, simulating the gradual drug elimination by the organism. New doses are periodically administered at time intervals  $\tau$ . So, the drug concentration at the capillary,  $\tilde{Q}(T)$ , is a function of time written as

$$\tilde{Q}(T) = \begin{cases} 0, & \text{if } T < T_0 \\ \tilde{Q}_0 \exp[-(T - l\tau)/T_x], & \text{if } T_0 + l\tau \leq T < T_0 + (l+1)\tau \end{cases}, \quad (7)$$

where  $l = 0, 1, 2, \dots$  is the number of applied doses,  $T_x$  is the characteristic time for the drug elimination by the organism and  $T_0$  is the time at which the treatment begins. The functional form of  $\tilde{Q}(T)$  is shown in Fig. 1.

As the nutrients, drugs diffuse from the capillary vessel toward the individual cells and their concentration  $Q(\vec{x}, t)$  at any lattice site at each time step is given by the stationary solution of the diffusion equation

$$\frac{\partial Q}{\partial t} = D_Q \nabla^2 Q - \Gamma^2 Q - \lambda_Q \Gamma^2 Q \sigma_c. \quad (8)$$

The first, second and third terms on the right hand side represent drug diffusion, natural degradation and absorption by cancer cells, respectively. Again, this equation is the simplest one describing the diffusion phenomenon. Eq. (8) is written using the same dimensionless variables of (1) and (2). Also, the parameters  $\tilde{Q}_0$  and  $D_Q$  can be made equal to the unity without generality loss. The boundary conditions are the same used for the nutrient fields, except at the capillary vessel where the concentration at each time step is given by Eq. (7).

Finally, a single change is introduced into the cell dynamics described in section II: an additional chance of death occurs whenever a cancer cell enters mitosis. Thus, every time a cancer cell divides, each one of the generated cells can die with probability

$$P_{del}^{(Q)}(\vec{x}) = 1 - \exp \left[ - \left( \frac{Q(\vec{x})}{\sigma_c(\vec{x}) \theta_{del}^{(Q)}} \right)^2 \right]. \quad (9)$$

The parameter  $\theta_{del}^{(Q)}$  controls the cell sensitivity to the drugs. Also, since in the original nutrient-limited model the normal cells do not take part on the cell dynamics, i. e., they do not divide or die, we disregard the chemotherapeutic effects on normal cells.

#### B. Results

The main aim of this work was to investigate the effects of treatments on the various morphologies, scaling and growth laws observed in the original model. Thus, for each morphology, determined by the fixed parameters reported in table I, the treatment parameters, namely,  $\tau$  (the dose period),  $\theta_{del}^{(Q)}$  (drug efficiency) and  $N_0$  (tumor size at the treatment beginning) were varied. Such parameters can be directly tested in the laboratory. The remaining parameters ( $\lambda_Q$ ,  $\Gamma$  and  $T_x$ ) associated to drug diffusion and elimination were also fixed in all the simulations.

In Fig. 2, the corresponding patterns for compact, papillary, and ramified morphologies with and without treatment are shown. In this figure the treatment is not able to cease tumor development. As can be seen, the morphological tumor patterns do not change under mild treatment. However, the regions occupied by the tumors are larger than those without treatment. These results

Morphology	$\lambda_N$	$\lambda_M$	$\lambda_Q$	$\alpha$	$\Gamma$	$\theta_{div}$	$\theta_{del}$	$T_\times$
Compact	25	10	10	$2/L$	$2/L$	0.3	0.03	4
Papillary	200	10	10	$2/L$	$2/L$	0.3	0.03	4
Ramified	200	10	10	$3/L$	$2/L$	0.3	0.01	4
Necrotic	50	25	10	$3/L$	$2/L$	0.3	0.03	4

TABLE I: Fixed parameters used in tumor growth simulations under chemotherapeutic treatment for each morphology type.

suggest that the direct attack to the tumor might be an inadequate treatment strategy. Indeed, the more invasive is the tumor, higher is the possibility of the cancer cells to reach the capillary vessel and, consequently, metastasize successfully. Such result is in agreement with the Israel's claim [31] that cancer cells trigger adaptation mechanisms in stress circumstances similar to those observed in bacterial colonies. Moreover, in our model neither genetic or epigenetic changes are necessary to explain the increase of tumor aggressiveness. It naturally emerges from the growth rules. A tumor submitted to successive chemotherapeutic treatments which do not lead to its complete eradication may progressively become more resistant, aggressive and malignant.

Very similar scaling laws  $R_g \sim n^\nu$  and  $S \sim n^\sigma$  for the treated tumors were observed ( $\nu$  and  $\sigma$  values are reported in [1]). The small differences in the exponents values for the number of tumor peripheral sites vanishes at the asymptotical limit of tumor size. This exponents invariance suggests that the fractal morphology is a robust aspect of these tumors and cannot be changed by small perturbations in the cell microenvironment. Obviously, the scaling laws for  $R_g$  and  $S$  are not defined for the tumors that cease their growth.

We have also studied the influence of the treatment parameters ( $\tau$ ,  $\theta_{del}^{(Q)}$ ,  $N_0$ ) on the tumor growth curves. In Fig. 3 the evolution in time of the total number of cancer cells for compact tumors is shown. Depending on dose period  $\tau$  the tumors may disappear, saturate their growth or progress according to power laws. Actually, the time interval between two consecutive doses is a fundamental clinical feature determining the treatment success. The power law regime observed when  $\tau$  is large means a slow progress, neatly contrasting with the exponential growth present in the Gompertz law describing tumor progress without chemotherapy. The tumor size at the beginning of the treatment is another important factor. Indeed, the exponents of the power laws characterizing the tumor growth are smaller when the initial tumor size is bigger. This scenario seems to be universal. Sometimes, as shown Fig. 3, compact tumors which began to receive drug doses at regular intervals of  $\tau = 5$  when it contained  $N_0 = 10^4$  cancer cells were eliminated slower than another one that began to be treated with  $N_0 = 5 \times 10^4$  cancer cells. However, this is not the rule. For example, simulations of papillary tumors indicate that smaller tumors are faster eliminated when  $\tau = 5$ . Finally, since the growth law

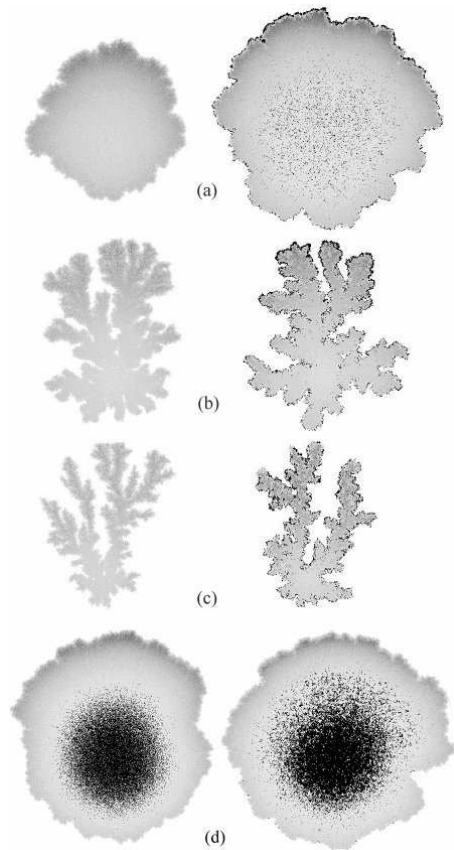


FIG. 2: Tumor growth patterns generated by the limited-nutrient model under chemotherapeutic treatment. The patterns are drawn in a gray scale where the darker gray regions represent higher cancer cell populations, the black points represent the sites occupied by necrotic cells, and the white regions represent the normal tissue. The tissue size is  $500 \times 500$ , and the initial “cancer seed” is 300 sites distant from the capillary. The total number of cancer cells depends on tumor morphology and reach up to  $2 \times 10^5$  for compact patterns. Two typical patterns, without (left) and with soft treatment (right) are shown, for (a) compact, (b) papillary, (c) ramified morphologies and (d) patterns with a necrotic core. The fixed parameters used to generate these morphologies are listed in table I. Mild treatment means that the period between two doses is large ( $\tau = 20$ ) and, therefore, the tumor grows continuously. The other parameters are  $\theta_{del}^{(Q)} = 0.1$  and  $N_0 = 10^4$ .

exponents depend on the parameter sets used, they are not universal. Concerning the  $\theta_{del}^{(Q)}$  parameter, it just modifies the treatment efficiency.

Fractal tumors are more resistant to treatments. In Fig. 4, the growth curves  $N_C \times T$  are drawn for compact, papillary, ramified and necrotic morphologies shown in Fig. 2. One can see that the more fractal is the tumor larger is the required time to eliminate it. Indeed, the lower growth rates of fractal tumors imply in a large fraction of cancer cells maintained at a quiescent state. So, since chemotherapeutic drugs considered in this model

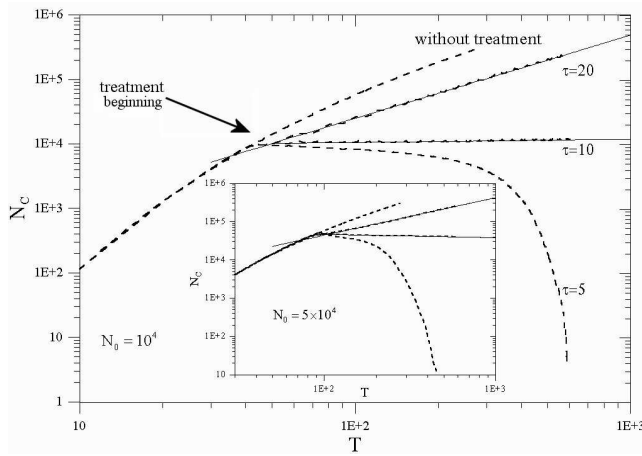


FIG. 3: Growth curves for compact patterns (dashed lines). Three dose intervals were tested ( $\tau = 5, 10, 20$ ) in tumors with two distinct initial sizes:  $N_0 = 10^4$  and  $N_0 = 5 \times 10^4$  (inset). The exponents of the power laws (slopes of the straight lines) are 1.3 (0.98) for the tumors with  $N_0 = 10^4$  ( $N_0 = 5 \times 10^4$ ) when  $\tau = 20$ , and 0.05 (-0.09) when  $\tau = 10$ .

only act in the dividing cells, the treatment becomes inefficient when the major fraction of the cancer cells are quiescent.

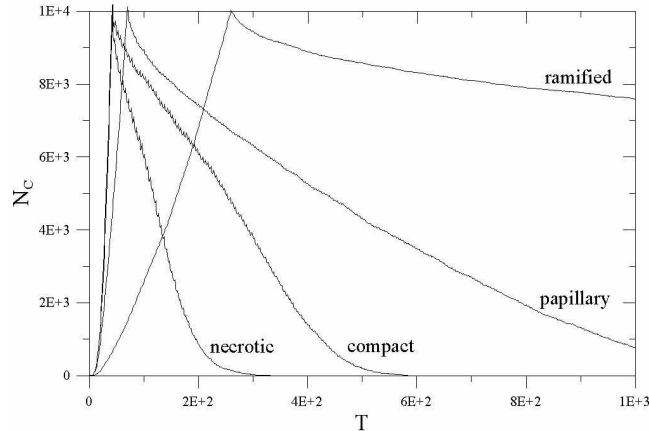


FIG. 4: Growth curves for distinct tumor morphologies. The doses were applied at intervals  $\tau = 5$  in tumors with initial sizes  $N_0 = 10^4$ .

In addition, we have studied tumor patterns exhibiting a central necrotic core. The results for cancer growth and the correspondent power laws are similar to those found for compact patterns. The density of cancer cells and their average division rates through the growth patterns are not significantly altered when the tumors are submitted to mild treatments (long time intervals between consecutive drug doses). Moreover, their growth patterns are very similar to those found in the untreated counterparts. Finally, tumors exhibiting necrotic cores are more easily eliminated when shorter periods of the drug administration are considered (Fig. 4).

#### IV. ANTIMITOTIC CHEMOTHERAPEUTIC DRUGS

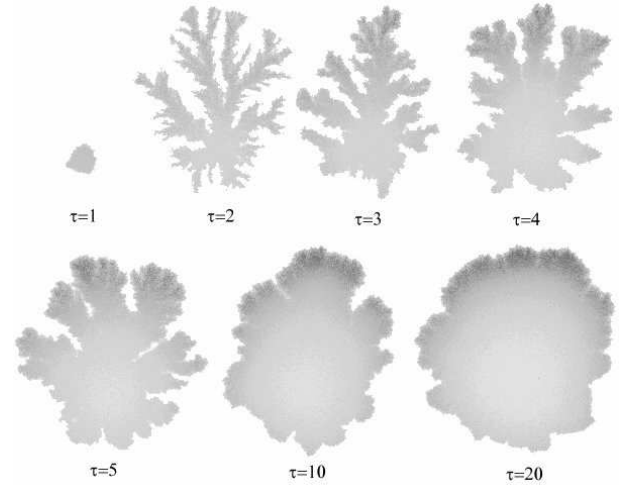


FIG. 5: Compact patterns under treatment with antimitotic drugs. The dose period  $\tau$  was varied and  $\theta_{div}^{(Q)} = 0.3$  was fixed. The other parameters are indicated in table I. Tumors become more and more fractal as the dose period decreases. At a critical period the tumors reach a frozen state in which their size remain constant during all the treatment.

Several drugs used in cancer chemotherapies do not kill cancer cells. Instead, they aim to stop the cell cycle in specific checkpoints. As a consequence of that, the tumors cease or slow down their growth rate. Examples of such drugs include the antimitotic agent Curacin A that blocks the cell cycle in the M-phase, mitomycin C, doxorubicin, and aclarubicin, among others [29]. In order to analyze the effects of drugs that inhibit cell division on tumor patterns, we introduce a very simple change in the cell dynamics of the model described in the previous section. Instead of an additional death probability given by Eq. (9), the division probability is modified by including an additional term in Eq. (3). So, the new division probability becomes

$$P_{div} = 1 - \exp \left[ - \left( \frac{N}{\sigma_c \theta_{div}} \right)^2 + \left( \frac{Q}{\sigma_c \theta_{div}^{(Q)}} \right)^2 \right], \quad (10)$$

in which the first and second terms in the exponential argument compete between themselves stimulating and inhibiting the cell mitosis, respectively. The parameter  $\theta_{div}^{(Q)}$  controls the drug influence on the cell division. Obviously, if the exponential argument is larger than the unity then  $P_{div} \equiv 0$ .

The biological interpretation of the present model is very distinct from that considered in the last section. Now, the drugs modify the intrinsic characteristics of the cancer cells and, consequently, the tumors must behave differently from those treated with cytotoxic agents. Indeed, as one can see in Fig. 5, a morphological transition

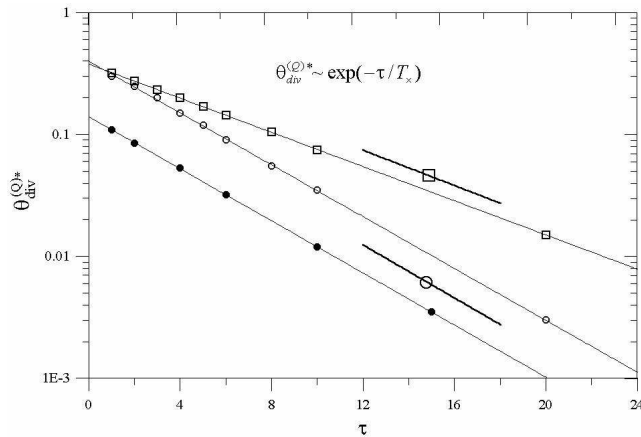


FIG. 6: Critical values  $\theta_{div}^{(Q)*}$  as a function of the dose period  $\tau$ . The symbols represent simulational data and the straight lines the respective exponential fittings. The open circles refer to the simulations using the parameters for the compact patterns listed in table I. The squares (filled circles) represent the same simulations except that  $T_x = 6$  ( $\theta_{div} = 0.1$ ). Also, the slopes  $1/4$  (circle) and  $1/6$  (square) are indicated. In order to estimate  $\theta_{div}^{(Q)*}$  we realized 20 independent simulations for each value of  $\theta_{div}^{(Q)}$  and considered that the growth failure for all these tentatives means tumor latency.

for the tumor patterns when the dose periods decrease is observed. If the period is sufficiently short the tumor size remains constant during the therapy. Obviously, the critical period depend on other model parameters, specially on  $\theta_{div}^{(Q)}$ . In order to see this dependence, was evaluated the critical value of  $\theta_{div}^{(Q)*}$  for which the tumors cease their growth with probability 1 as a function of  $\tau$ . A mean field analysis of Eq. (10) provides  $\theta_{div}^{(Q)} \sim \exp(-\tau/T_x)$ , in agreement with the simulations as indicated in Fig. 6. Thus, it was found an exponential decay with an universal characteristic length  $T_x$  that is independent of the other model parameters. This law, relating two important clinical parameters, is valid for an wide set of parameter values. In addition to the compact tumors shown in figure 5, it was also simulated papillary tumors under antimitotic treatment, and a similar morphology transition was observed.

Fig. 7 shows that these morphological transitions occurred at well defined  $\theta_{div}^{(Q)}$  values. Near the critical value, instabilities in the reaction-diffusion equations lead to a branching growth [15]. Below this threshold the cell death rate equals cell division, and the tumor growth effectively stops. This qualitative behavior near the transition will probably not be observed in experimental tumors, since a very reliable determination of  $\theta_{div}^{(Q)}$  is very difficult. On the other hand, experiments exhibiting both regimes, above and below the critical value, are realizable today, due to the great advances in drug delivery control. Such assays might corroborate the complex behaviors predicted by our model.

The antimitotic treatment affects both the growth and

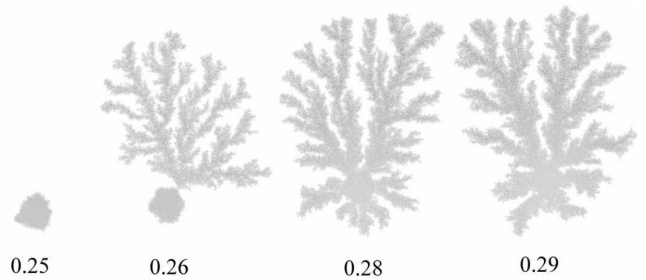


FIG. 7: Morphological transitions at  $\theta_{div}^{(Q)*}$ . The patterns were originally compact and the model parameters are listed in table I. The dose period was fixed at  $\tau = 2$  and  $\theta_{div}^{(Q)}$  varied around its critical value.

scaling laws. The compact patterns in the original model, for which the gyration radius and number of occupied sites on the tumor border scale as the square root of the total number of occupied sites (i. e.  $\nu = \sigma = 1/2$ ), become progressively more fractal as the dose intervals are decreased. Consequently, it was obtained  $\nu > 1/2$  and  $\sigma > 1/2$  indicating fractal tumors with a fractal dimension given by  $d_f = 1/\nu$ . In general, all the tumors become more fractal when submitted to antimitotic treatments. So, there is a neat contrast with the invariance of the fractal dimension of the growing tumors under the cytotoxic treatment described in the previous section. In Fig. 8 the increase in the number of cancer cells relative to the treatment beginning ( $N_C - N_0$ ) is plotted, for distinct dose intervals, as a function of the time afterwards the treatment beginning ( $T - T_0$ ). These curves suggest power laws for the time evolution of the number of cancer cells with a weak dependence on the  $\tau$  parameter. Indeed, we have  $(N_C - N_0) \sim (T - T_0)^\beta$  whit  $\beta \in [1.2, 1.4]$ . As  $\tau$  decreases, the number of tumor cells initially decays for a while, but subsequently recovers its growth (inset of Fig. 8). Below a given dose interval,  $N_C$  decreases monotonically up to a constant value.

In order to analyze the cell division rates through the tumor, we computed the average cancer cell density ( $\langle \sigma_c \rangle$ ) and cell division rate ( $w_{div}$ ) along a longitudinal cut across the growth pattern. These average values were plotted as a function of the distance from the capillary vessel. In Fig. 9 these plots are shown for compact patterns treated with distinct  $\tau$  values. For larger  $\tau$  values (Fig. 9(a)) both, division rate and cancer cell density, have sharp maxima on the tumor border in front and opposite to the capillary vessel. Notice that the peaks for division rate are significantly narrower than those for cancer cell density, demonstrating that the proliferative fraction of the tumor comprises just a small rim located at the tumor border. As the treatment is intensified (shorter  $\tau$  values are considered) the cell densities through the tumors become more uniform, whereas the division rates continue exhibiting sharp maxima at the tumor borders (Figs. 9(b) and (c)). If  $\tau$  is sufficiently short in order to halt the tumor growth, the division rates and cancer densities become uniform along the tu-

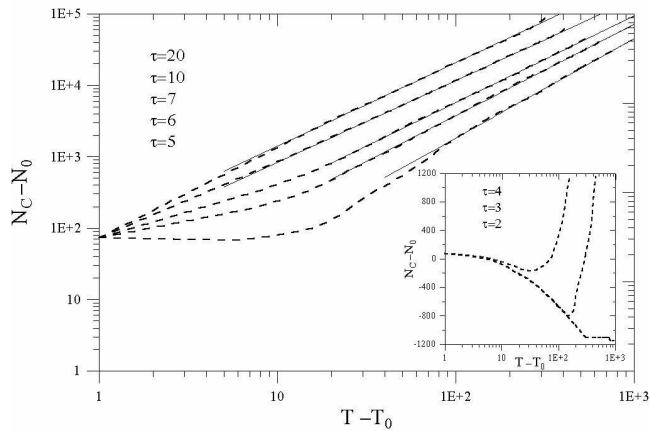


FIG. 8: Growth curves (dashed lines) for the papillary patterns under antimetabolic therapy. The dose intervals used were  $\tau = 20, 10, 7, 6, 5, 4, 3, 2$  and the upper curves represent the larger intervals. For the larger dose intervals ( $\tau \geq 5$ ) the tumor growth follows power laws with exponents in the range [1.2,1.4]. For shorter intervals ( $\tau \leq 4$ ), the curves are shown in a semi-log plot (inset). In these simulations  $\theta_{div}^{(Q)} = 0.3$  was used in addition to the parameters of table I.

mor (Fig. 9(d)). So, in these cases the division rates are counterbalanced by the death rates, leading to a vanishing net rate of cancer growth. All these results show that the tumor patterns are altered when the mitotic properties of the cancer cells are modified by external agents.

## V. CONCLUSIONS

In the present work, a reaction-diffusion model to simulate the effects of chemotherapies on the growth of carcinomas “in situ” have been studied. The model includes cell death and division, competition among cancer and normal cells by nutrients and periodical drug administration. Two kinds of chemotherapies, using cytotoxic and antimetabolic drugs, were modelled.

In the cytotoxic model the tumors can be completely eradicated, cease their growth or grow continuously. The last case occurs when the treatment is inefficient or the intervals between consecutive doses of drugs are large. Moreover, the morphologies and scaling laws of the growing tumor patterns are preserved. In contrast, for therapeutic approaches using antimetabolic agents a morphological transition in the tumor patterns was observed. The growth patterns become progressively more fractal

as more effective treatments (shorter intervals between consecutive doses and/or more efficient drugs) are considered.

Such morphological transitions are similar to recent studies claiming that bacterial colonies exposed to non-lethal concentrations of antibiotics exhibit drastic changes in their growth patterns [32]. For bacteria, these changes were imputed to variations in bacterial properties such as metabolic load and chemotaxis. In turn, normal and cancer cells cultured in monolayer and collagen gel exhibit a dynamical transition in their aggregation regimes as an adaptive response to the growth constraints imposed by high cell population density or long permanence in culture [33]. Again, the results obtained in the present work are in agreement with the point of view that cancer cells can develop an integrated defense program against stress situations similar to the response of bacterial colonies facing severe and sustained threats [31]. However, as far as we are concerned, there are no reports on cancer literature concerning transitions morphologies in the histological patterns of tumors submitted to chemotherapy. Thus, formal models like the one proposed in this paper, generally not familiar for the most of the biomedical researchers [34], can guide and refine new experiments intended to analyze such morphological transitions. Currently, experiments “in vitro” with cancer cells are being performed in our laboratories in order to investigate those morphological transitions.

It is important to mention that, usually, real effective treatments employ several therapeutic methods simultaneously [27]. So, a more realistic chemotherapeutic model should consider combined cytotoxic and antimetabolic treatments. Nevertheless, in these cases relevant features such as the robustness of the tumors fractal scaling and the morphology transitions can be masked. At last, we are modelling others cancer therapeutic strategies, such as virus and immunotoxins therapies, as well as the combination of distinct treatments by using reaction-diffusion models like that considered in this paper.

## Acknowledgments

S.C. Ferreira Jr. would like to thank the UFV Physics Department (Viçosa, Brazil) for the welcoming hospitality and the Professor J. G. Moreira (Departamento de Física, UFMG, Brazil) for fruitful discussions. This work was partially supported by the CNPq and FAPEMIG - Brazilian agencies.

[1] S. C. Ferreira Jr., M. L. Martins, and M. J. Vilela, Phys. Rev. E **65** 021907 (2002).  
 [2] D. Hanahan and R. A. Weinberg, Cell **100**, 57 (2000).  
 [3] J. O. D. Mc Gee, P. G. Isaacson, and N. A. Wright, Oxford Textbook of Pathology, Oxford University Press (1992).

[4] R. A. Weinberg, Sci. Am. **275**, 32 (1996).  
 [5] W. H. Clark, J. Cancer **64**, 631 (1991).  
 [6] G. I. Evan and K. H. Vousden, Nature **411**, 342 (2001).  
 [7] L. J. Old, Sci. Am. **275**, 136 (1996).  
 [8] J. Gómez-Navarro, D. T. Curiel, and J. T. Douglas, Eur.



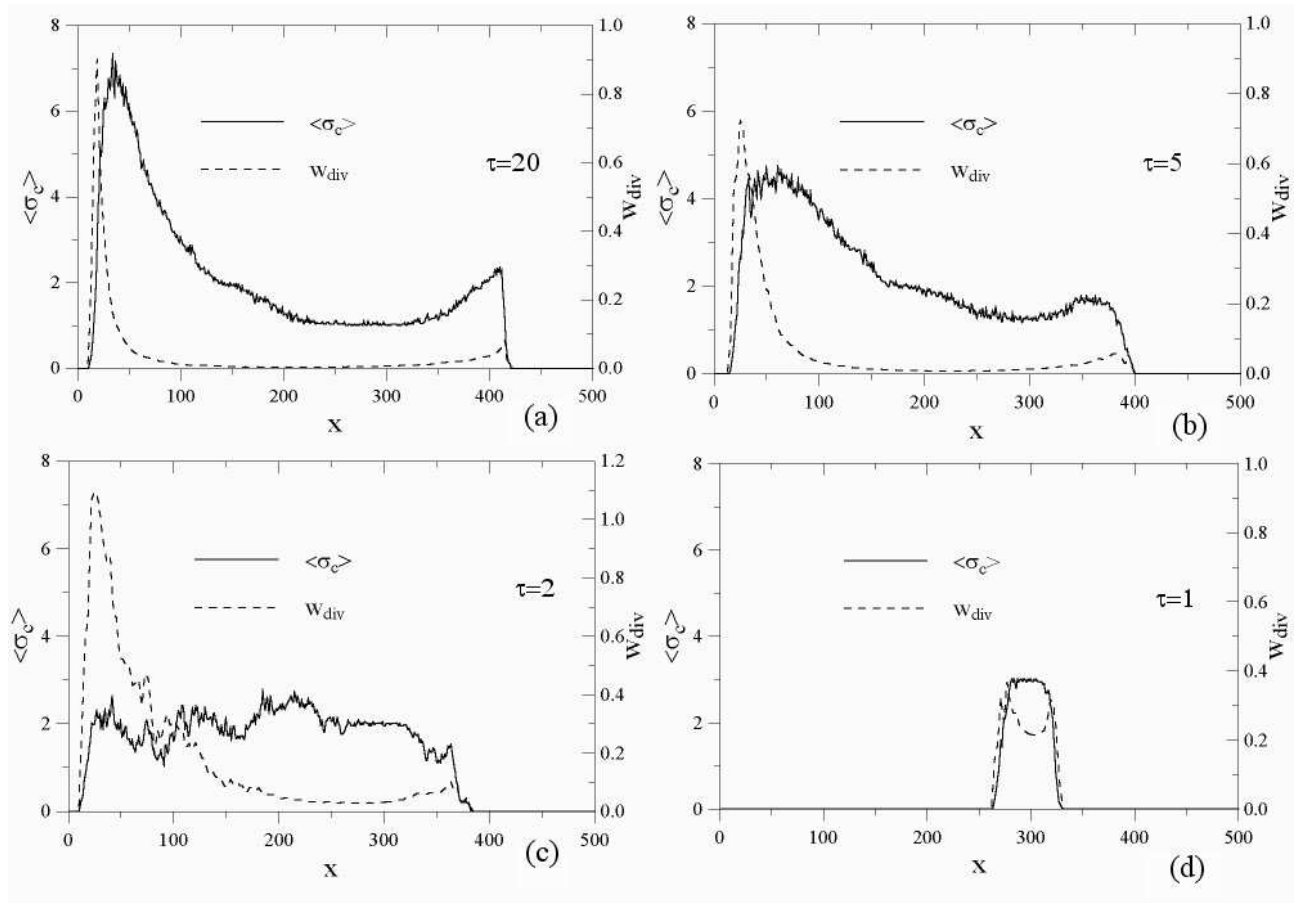


FIG. 9: Density of cancer cells  $\sigma_c$  (continuous lines) and division rates  $w_{div}$  (dashed lines) as a function of the distance from the capillary vessel along a longitudinal cut of the tumor. The fixed model parameters are those referent to the compact morphology indicated in table I and  $\theta_{div}^{(Q)} = 0.3$ . The plots correspond to (a)  $\tau = 20$ , (b)  $\tau = 5$ , (c)  $\tau = 2$  and (d)  $\tau = 1$ . The left and right vertical axes represent  $\sigma_c$  and  $w_{div}$ , respectively.

- J. Cancer **35**, 867 (1999).
- [9] J. Folkman, Sci. Am. **275**, 150 (1996).
- [10] J. R. Bischoff, *et. al.*, Science **274**, 373 (1996).
- [11] G. J. Pettet, C. P. Please, M. J. Tindall, and D. L. S. McElwain, Bull. Math. Biol. **63**, 231 (2001).
- [12] N. Bellomo and L. Preziosi, Mathl. Comp. Modelling **32**, 413 (2000).
- [13] H. A. Levine, S. Pamuk, B. D. Sleeman, and M. Nilsen-Hamilton, Bull. Math. Biol. **63**, 801 (2001).
- [14] E. De Angelis and L. Preziosi, Math. Models Meth. in Appl. Sci. **10**, 379 (2000).
- [15] L. M. Sander and T. S. Deisboeck, Phys. Rev. E **66**, 051901 (2002).
- [16] M. Scalerandi, A. Romano, G. P. Pescarmona, P. P. Del-santo, and C. A. Condat, Phys. Rev. E **59**, 2206 (1999).
- [17] M. Scalerandi, B. Capogrosso, Sansone, C. Benati, and C. A. Condat, Phys. Rev. E **65**, 051918 (2002).
- [18] B. Capogrosso Sansone, M. Scalerandi e C. A. Condat, Phys. Rev. Lett. **87**, 128102 (2001).
- [19] S. C. Ferreira Jr., M. L. Martins, and M. J. Vilela, Physica A **261**, 569 (1998).
- [20] S. C. Ferreira Jr., M. L. Martins, and M. J. Vilela, Physica A **272**, 245 (1999).
- [21] F. Kozusco, Pao-Hsiu Chen, S. G. Grant, B. W. Day, and J. Carl Panetta, Math. Biosci. **170**, 1 (2001).
- [22] F. Montalenti, G. Sena, P. Cappella, and P. Ubezio, Phys. Rev. E **57**, 5877 (1998).
- [23] R. K. Sachs, L. R. Hlatky, and P. Hahnfeldt, Mathl. Compt. Modelling **33**, 1297 (2001).
- [24] J. T. Wu, H. M. Byrne, D. H. Kirn, and L. M. Wein, Bull. Math. Biol. **63**, 731 (2001).
- [25] M. Scalerandi and B. C. Sansone, Phys. Rev. Lett. **89**, 218101 (2002).
- [26] T. L. Jackson and H. M. Byrne, Math. Biosci. **164**, 17 (2000).
- [27] S. Hellman and E. E. Volkes, Sci. Am. **275**, 118 (1996).
- [28] J. C. Panetta, Bull. Math. Biol. **58**, 425 (1996).
- [29]
- [30] R. K. Jain, Sci. Am. **271**, 58 (1994).
- [31] L. Israel, J. Theor. Biol. **178**, 375 (1996).
- [32] E. Ben-Jacob, I. Cohen, I. Golding, D. L. Gutnick, M. Tcherpakov, D. Helbing, and I. G. Ron, Physica A **282**, 247 (2000).
- [33] R. L. Mendes, A. A. Santos, M. L. Martins, and M. J. Vilela, Physica A **298**, 471 (2001).
- [34] The Prostate Cancer Complexity Working Group, Complexity **7**(5), 22 (2002).